IEEE Transactions on Power Electronics, pp. 1–11, 2024

Stability Analysis of Input-Series/Output-Parallel Solid-State Transformers Equipped with Second-Order Harmonic Active Power Filters

A. Cervone, T. Wei, and D. Dujic

POWER ELECTRONICS LABORATORY
ÉCOLE POLYTECHNIQUE FÉDÉRALE DE LAUSANNE

This article has been accepted for publication in IEEE Transactions on Power Electronics. This is the author's version which has not been fully edited and content may change prior to final publication. Citation information: DOI 10.1109/TPEL.2024.3351314

Stability Analysis of Input-Series/Output-Parallel Solid-State Transformers Equipped with Second-Order Harmonic Active Power Filters

Andrea Cervone, *Member, IEEE*, Tianyu Wei, *Student Member, IEEE*, and Drazen Dujic, *Senior Member, IEEE*

***Abstract*—Solid-State Transformers with Input-Series/Output-Parallel configuration offer a convenient solution for AC/DC conversion due to their scalability and modularity. In this configuration, each module experiences a second-order harmonic ripple caused by local single-phase AC/DC conversion. To neutralize this ripple, Active Power Filters can be installed, eliminating the need for oversized DC-bus capacitances. However, the presence of multiple APFs, working at the same time, can lead to dynamic interactions and potential instability due to the coupling between different ISOP SST modules. This study examines the mutual dynamics arising from multiple APFs in ISOP SSTs. It is shown that ensuring stability for the operation of a single APF does not automatically guarantee the overall stability when all APFs are simultaneously enabled. To study this phenomenon, an analysis approach based on the Generalized Nyquist Criterion for Multi-Input/Multi-Output systems is derived. Through the proposed approach, the closed-loop stability only needs to be verified towards two equivalent SST impedances that intrinsically considers the mutual coupling. This provides a simple design and verification tool for the APF controller, and the results are validated experimentally using a single-phase ISOP SST.**

***Index Terms*—Input-Series/Output-Parallel (ISOP), Solid-State Transformer (SST), Active Power Filter (APF), Multi-Input/Multi-Output (MIMO) Stability.**

I. Introduction

SOLID State Transformers (SSTs) have recently emerged as a promising solution to offer efficient, reliable, and flexible power conversion in many different application areas, ranging from renewable energy integration to industrial applications and traction [1]–[6]. They are aimed at offering the same characteristics as conventional power transformers (e.g., voltage/current scaling, galvanic insulation, etc...) with the improved benefits offered by power electronics in terms of enhanced controllability and increased flexibility, and with the possibility to be employed not only for AC/AC conversion, but also in DC/DC and hybrid AC/DC systems.

Among various SST configurations, the Input-Series/Output Parallel (ISOP) architecture has attracted significant attention thanks to its scalability and modularity. In an ISOP SST, multiple modules are connected in series on the primary side to achieve high voltage ratings, and in parallel on the secondary side to achieve high current ratings [1], [2], [4]–[6].

All authors are with the Power Electronics Laboratory (PEL) of the École Polytechnique Fédérale de Lausanne (EPFL), Lausanne, Switzerland.

In case of AC/DC conversion, each ISOP SST module typically incorporates a dedicated single-phase AC/DC conversion stage. However, as known, their operation introduces a power oscillation at twice the AC line frequency, that could adversely affect the DC-bus voltage of each module and, in single-phase configurations, may even propagate to the secondary side of the overall converter [7].

The mitigation of the second-order harmonic could be accomplished by installing large capacitor banks or employing LC trap filters, that could potentially completely eliminate the ripple. However, due to the relatively low frequency of the oscillating power (e.g., 100 Hz, 120 Hz, or 33.3 Hz for AC systems operating at 50 Hz, 60 Hz, or 16.7 Hz, respectively), these passive solutions result in increased system bulkiness, thereby impacting the overall dimensions, weight, and, consequently, power density of the converter [8].

An alternative approach consists in employing Active Power Filters (APFs) as supplementary power electronic conversion structures that are controlled to counteract the power ripple resulting from the single-phase AC/DC conversion [9]–[13] (see Fig. 1). In the presence of APFs, there is no need to size the DC bus capacitors of the ISOP SST modules for second-order harmonic ripple suppression. Instead, they can be downsized to enhance the overall system's compactness.

Each APF can be designed to locally counteract the second-order harmonic voltage of the module where it is installed, employing a closed-loop control selectively acting on a single frequency of interest. However, in the context of ISOP

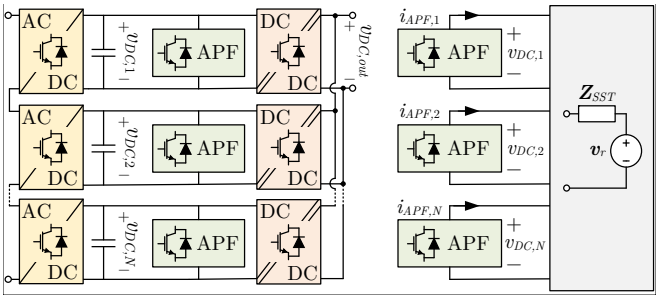

Fig. 1. Schematic representation of an ISOP SST equipped with Active Power Filters (left) and modeling of the SST as a Multi-Input/Multi-Output Thevenin equivalent circuit seen from the DC-bus ports (right).

This article has been accepted for publication in IEEE Transactions on Power Electronics. This is the author's version which has not been fully edited and content may change prior to final publication. Citation information: DOI 10.1109/TPEL.2024.3351314

configurations, it is important to note that all the modules of the SST are intricately interconnected, creating dynamic coupling effects. This means that the SST effectively behaves as a dynamical interconnection network, and each APF may affect not only the module where it is installed, but also all the others [14].

This mutual interaction among the SST modules has been explored in [14], primarily focusing on its impact on the steady-state operating conditions. It has been shown that the coupling between the SST modules may lead to some resonances in the system and, when only a subset of the APFs is in operation, the effects on some DC-bus voltages may be even worse than in case when all APFs are inoperative.

This work goes a step further and puts its emphasis on the dynamical performance aspects and on their implication for the system stability. In what follows, it is demonstrated that ensuring the stable closed-loop operation of each individual APF alone is insufficient to guarantee overall system stability when multiple APFs operate concurrently. Instead, it becomes imperative to establish more stringent requirements for the closed-loop system as a whole.

In the proposed approach, the ISOP SST is analyzed as a Multi-Input/Multi-Output (MIMO) dynamical system, and the mutual interactions between different modules are mathematically formulated through an equivalent impedance matrix. Then, based on the Generalized Nyquist Criterion (GNC), a simplified approach is developed to assess the overall system stability, which relies on the analysis of the APF controller when interacting in feedback with only two equivalent impedances, that are inherently including the impact of mutual coupling effects within the SST.

The rest of the paper is structured as follows. First, Section II introduces the mathematical model of the ISOP SST as an equivalent MIMO system. Then, the closed-loop stability analysis is discussed in Section III, which first deals with the isolated operation of a single APF, and then examines the simultaneous operation of all units. The stability analysis using the GNC and the simplified approach are also explained in the same Section. Afterwards, Section IV presents the analyzed setup and provides an example how the equivalent impedances of an ISOP SST can be evaluated using a simplified equivalent circuit. The experimental validation of the proposed approach is presented in Section V. It is proven and verified that even when an APF is stable when operating independently from others, some instabilities may occur when multiple units are operating at once, which can be predicted by the proposed analysis approach. Finally Section VI summarizes the conclusions of this work.

II. Mathematical Model

The analyzed architecture is an ISOP SST composed of N identical conversion modules. Each module is composed of an AC/DC conversion stage, a local DC-bus capacitance, and an isolated DC/DC conversion stage. An APF is connected in parallel to the DC-bus terminals of each module. The schematic representation of the circuit is shown in Fig. 1.

In what follows, the DC-bus voltage of each floating module of the SST is denoted as $v_{DC,k}$ (with $k = 1, \dots, N$), while the output voltage of the overall SST, which is common to all modules in the ISOP configuration, is denoted as $v_{DC,out}$. In absence of any APF, the DC-bus of any k-th conversion module is affected by a second-order harmonic ripple, and the corresponding voltage is denoted as $v_{r,k}$.

By installing an APF on the k-th SST module, it is possible to inject a controlled current $i_{APF,k}$ on the corresponding DC-bus. This current can be used to affect the DC-bus voltage $v_{DC,k}$ in a way to contrast the second-order harmonic ripple and make $v_{DC,k}$ differ from $v_{r,k}$. However, due to the mutual coupling existing between different modules in the ISOP configuration (which is mainly due to the effect of the DC/DC conversion stages), the current $i_{APF,k}$ can also alter the DC-bus voltages of the other SST modules $v_{DC,h}$ (with $h \neq k$).

In the linear approximation, the relationship between the DC-bus voltages and the APF currents can be expressed in the Laplace domain as:

$$\underbrace{\begin{bmatrix} v_{DC,1} \\ v_{DC,2} \\ \vdots \\ v_{DC,N} \end{bmatrix}}_{\boldsymbol{v}_{DC}(s)} = \underbrace{\begin{bmatrix} v_{r,1} \\ v_{r,2} \\ \vdots \\ v_{r,N} \end{bmatrix}}_{\boldsymbol{v}_{r}(s)} - \underbrace{\begin{bmatrix} Z_{1,1} & Z_{1,2} & \cdots & Z_{1,N} \\ Z_{2,1} & Z_{2,2} & \cdots & Z_{2,N} \\ \vdots & \vdots & \ddots & \vdots \\ Z_{N,1} & Z_{N,2} & \cdots & Z_{N,N} \end{bmatrix}}_{\boldsymbol{Z}_{SST}(s)} \cdot \underbrace{\begin{bmatrix} i_{APF,1} \\ i_{APF,2} \\ \vdots \\ i_{APF,N} \end{bmatrix}}_{\boldsymbol{i}_{APF}(s)} \quad (1)$$

where the explicit dependence on the Laplace complex variable s has been omitted for notation compactness. The expression (1) can be interpreted as a Multi-Input/Multi-Output (MIMO) Thevenin equivalent of the ISOP SST, seen from DC-bus terminals of each module, as schematically represented in the right plot of Fig. 1.

The impedance $Z_{k,h}(s)$ identifies the effect of the APF current $i_{APF,k}(s)$ on the DC-bus voltage $v_{DC,h}(s)$. In the reasonable assumption that all SST modules are identical, it results that:

$$Z_{k,k}(s) = Z_A(s) \quad (\text{with } k = 1, \dots, N) \quad (2)$$

$$Z_{k,h}(s) = Z_M(s) \quad (\text{with } k, h = 1, \dots, N, \text{ and } k \neq h) \quad (3)$$

where the impedance $Z_A(s)$ represents a self-induced contribution of each module, while $Z_M(s)$ identifies the mutual influence of different modules. Therefore, the equivalent impedance matrix $\boldsymbol{Z}_{SST}(s)$ is symmetric, and equal to:

$$\boldsymbol{Z}_{SST}(s) = \begin{bmatrix} Z_A & Z_M & \cdots & Z_M \\ Z_M & Z_A & \cdots & Z_M \\ \vdots & \vdots & \ddots & \vdots \\ Z_M & Z_M & \cdots & Z_A \end{bmatrix} \quad (4)$$

III. Stability Analysis

As previously mentioned, the role of each APF is to absorb a controlled current from the corresponding DC-bus terminals, in a way to contrast the second-order harmonic ripple introduced by the AC/DC conversion stages. In absence of a centralized control, the current $i_{APF,k}$ is computed only

This article has been accepted for publication in IEEE Transactions on Power Electronics. This is the author's version which has not been fully edited and content may change prior to final publication. Citation information: DOI 10.1109/TPEL.2024.3351314

from the measured DC-bus voltage $v_{DC,k}$. In linearity, the relationship can be expressed in the Laplace domain as:

$$i_{APF,k}(s) = Y_{APF}(s) \cdot v_{DC,k}(s) \tag{5}$$

The controller transfer function $Y_{APF}(s)$ can be interpreted as an equivalent admittance connected in parallel to the DC-bus terminals of the k-th SST module. If $Y_{APF}(j\omega)$ has an infinite magnitude at the frequency $2\omega_{AC}$ of the harmonic injection, the APF would mimic the effect of an ideal trap filter, and the corresponding voltage ripple $v_{DC}(j2\omega_{AC})$ can be perfectly neutralized in steady-state conditions. On the contrary, the APF should have negligible effect at all other frequencies, and it should especially have no influence on the DC voltage. Therefore, $Y_{APF}(s)$ can be realized to include a resonant behavior at $2\omega_{AC}$, and to be zero for $\omega = 0$.

A. Stability of a single Active Power Filter

When a single APF is enabled, it results that:

$$\begin{aligned} v_{DC,k}(s) &= v_{r,k}(s) - Z_A(s) \cdot i_{APF,k}(s) = \\ &= v_{r,k}(s) - Z_A(s) \cdot Y_{APF}(s) \cdot v_{DC,k}(s) \end{aligned} \tag{6}$$

meaning that the voltage $v_{DC,k}$ on the corresponding DC-bus terminals is given by

$$v_{DC,k}(s) = \underbrace{\frac{1}{1 + Z_A(s) \cdot Y_{APF}(s)}}_{S_{APF}(s)} \cdot v_{r,k}(s) \tag{7}$$

Therefore, the stability of a single APF connected to the SST can be analyzed from the poles of the sensitivity function $S_{APF}(s) = 1/[1 + Z_A(s) \cdot Y_{APF}(s)]$. As known, this can be done by studying the open loop transfer function $L(s) = Z_A(s) \cdot Y_{APF}(s)$ through the Nyquist stability criterion. By knowing the impedance $Z_A(s)$, the APF controller $Y_{APF}(s)$ can be designed to achieve the desired performances while providing acceptable gain and phase margins.

B. Stability of multiple Active Power Filters

By considering the case where all APFs are enabled, the vector $\boldsymbol{i}_{APF}(s)$ in (1) can be expressed as:

$$\underbrace{\begin{bmatrix} i_{APF,1} \\ i_{APF,2} \\ \vdots \\ i_{APF,N} \end{bmatrix}}_{\boldsymbol{i}_{APF}(s)} = \underbrace{\begin{bmatrix} Y_{APF} & 0 & \cdots & 0 \\ 0 & Y_{APF} & \cdots & 0 \\ \vdots & \vdots & \ddots & \vdots \\ 0 & 0 & \cdots & Y_{APF} \end{bmatrix}}_{\boldsymbol{Y}_{APF}(s)} \cdot \underbrace{\begin{bmatrix} v_{DC,1} \\ v_{DC,2} \\ \vdots \\ v_{DC,N} \end{bmatrix}}_{\boldsymbol{v}_{DC}(s)} \tag{8}$$

By combining (1) and (8), it can be derived that:

$$\begin{aligned} \boldsymbol{v}_{DC}(s) &= \boldsymbol{v}_r(s) - \boldsymbol{Z}_{SST}(s) \cdot \boldsymbol{i}_{APF}(s) = \\ &= \boldsymbol{v}_r(s) - \boldsymbol{Z}_{SST}(s) \cdot \boldsymbol{Y}_{APF}(s) \cdot \boldsymbol{v}_{DC}(s) \end{aligned} \tag{9}$$

which can be rearranged to get

$$\boldsymbol{v}_{DC}(s) = \underbrace{\left[\boldsymbol{I} + \boldsymbol{Z}_{SST}(s) \cdot \boldsymbol{Y}_{APF}(s)\right]^{-1}}_{\boldsymbol{S}(s)} \cdot \boldsymbol{v}_r(s) \tag{10}$$

The expression (10) is the MIMO counterpart of (7), and the open-loop transfer matrix $\boldsymbol{L}(s) = \boldsymbol{Z}_{SST}(s) \cdot \boldsymbol{Y}_{APF}(s)$ affects the stability by determining the poles of the sensitivity matrix $\boldsymbol{S}(s) = \left[\boldsymbol{I} + \boldsymbol{Z}_{SST}(s) \cdot \boldsymbol{Y}_{APF}(s)\right]^{-1}$. Since (10) is a matrix expression, it means that all the N installed APFs interact with the SST and can potentially influence one another.

Given the symmetry property (4) of $\boldsymbol{Z}_{SST}(s)$, it can be proven that the sensitivity matrix also shows a similar symmetry, and can be expressed as:

$$\boldsymbol{S}(s) = \begin{bmatrix} S_A & S_M & \cdots & S_M \\ S_M & S_A & \cdots & S_M \\ \vdots & \vdots & \ddots & \vdots \\ S_M & S_M & \cdots & S_A \end{bmatrix} \tag{11}$$

with $S_A(s)$ and $S_M(s)$ being expressed as in (12)-(13).

To guarantee the stability of the SST with the simultaneous functioning of all APFs, both $S_A(s)$ and $S_M(s)$ should be stable. However, as can be seen from (12)-(13), their expressions depend on both $Z_A(s)$ and $Z_M(s)$. Only if $Z_M(s) = 0$ (i.e., in absence of any mutual interaction), then $S_M(s) = 0$ and the expression of $S_A(s)$ is equivalent to (7), meaning that the ISOP SST behaves as N independent modules that can be studied individually. In all other cases, the mutual influence of the modules cannot be neglected, and this means that guaranteeing the stability of a single APF in operation (which is assessed from (7)) is not enough to automatically guarantee the stability of the system with N APFs. Indeed, dynamically interactions may arise between different modules through the effect of the mutual inductance $Z_M(s)$.

C. Stability Analysis with the Generalized Nyquist Criterion

The expressions (12)-(13) can be used to evaluate the stability of the SST with all the APFs in operation. However, those expressions are way too complicated to be used for the design of the APF controller $Y_{APF}(s)$. Therefore, an alternative approach is developed in the following.

By considering the coupling of the SST and of all the APFs as a MIMO dynamical system, the stability can be assessed by applying the Generalized Nyquist Criterion (GNC). Among different equivalent formulations of the GNC, the one used in this work is based on the evaluation of the eigenvalues of the loop gain transfer matrix $\boldsymbol{L}(s) = \boldsymbol{Z}_{SST}(s) \cdot \boldsymbol{Y}_{APF}(s)$ (which, it is worth emphasizing, are N transfer functions

$$S_A(s) = \frac{[Y_{APF} Z_A + (N-2) \cdot Y_{APF} Z_M + 1]}{[1 + Y_{APF} Z_A] \cdot [Y_{APF} Z_A + (N-2) \cdot Y_{APF} Z_M + 1] - (N-1) \cdot [Y_{APF} Z_M]^2} \tag{12}$$

$$S_M(s) = \frac{-[Y_{APF} Z_M]}{[1 + Y_{APF} Z_A] \cdot [Y_{APF} Z_A + (N-2) \cdot Y_{APF} Z_M + 1] - (N-1) \cdot [Y_{APF} Z_M]^2} \tag{13}$$

(the explicit dependence of Z_A, Z_M and Y_{APF} on the Laplace complex variable s has been omitted for notation compactness)

This article has been accepted for publication in IEEE Transactions on Power Electronics. This is the author's version which has not been fully edited and content may change prior to final publication. Citation information: DOI 10.1109/TPEL.2024.3351314

depending on the Laplace complex variable s, sometimes referred to as eigenloci) [16].

To be more specific, the GNC states that the stability of the closed-loop system $\boldsymbol{S}(s) = \left[\boldsymbol{I} + \boldsymbol{Z}_{SST}(s) \cdot \boldsymbol{Y}_{APF}(s)\right]^{-1}$ can be assessed by observing the Nyquist plot of the eigenvalues of $\boldsymbol{L}(s)$. Since $\boldsymbol{L}(s)$ does not have poles with positive real part, if the Nyquist plot of all its eigenvalues do not encircle the critical point $(-1 + j0)$ of the complex plane, then the closed-loop system $\boldsymbol{S}(s)$ is stable [16].

Considering that $\boldsymbol{Y}_{APF}(s)$, as expressed in (8), is a diagonal matrix with all terms being equal, the eigenvalues of the open-loop transfer matrix $\boldsymbol{L}(s) = \boldsymbol{Z}_{SST}(s) \cdot \boldsymbol{Y}_{APF}(s)$ can be easily found from the eigenvalues of the impedance matrix $\boldsymbol{Z}_{SST}(s)$. Indeed, if $Z_\lambda(s)$ is used to denote an arbitrarily chosen eigenvalue of $\boldsymbol{Z}(s)$ and $\boldsymbol{x}_\lambda(s)$ is a corresponding eigenvector, then, by definition:

$$\boldsymbol{Z}_{SST} \cdot \boldsymbol{x}_\lambda = Z_\lambda \cdot \boldsymbol{x}_\lambda \tag{14}$$

and, if the same vector $\boldsymbol{x}_\lambda(s)$ is multiplied by $\boldsymbol{L}(s)$, by combining (8) with (14), it results:

$$\begin{aligned} \boldsymbol{L} \cdot \boldsymbol{x}_\lambda &= \boldsymbol{Z}_{SST} \cdot \boldsymbol{Y}_{APF} \cdot \boldsymbol{x}_\lambda = \\ &= Z_\lambda \cdot Y_{APF} \cdot \boldsymbol{x}_\lambda = L_\lambda \cdot \boldsymbol{x}_\lambda \end{aligned} \tag{15}$$

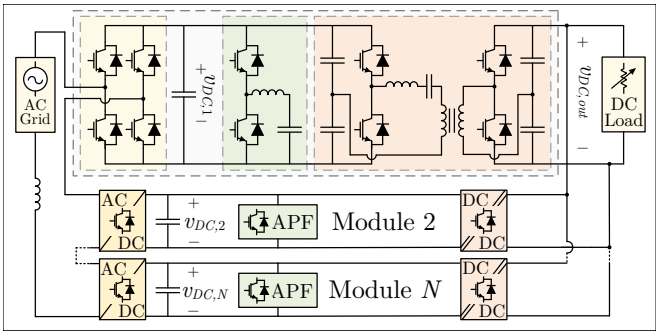

Fig. 2. The Power Electronics Traction Transformer (PETT), analyzed as example of an ISOP SST: Top) Circuit Topology; Bottom) Experimental setup.

This means that $L_\lambda(s) = Z_\lambda(s) \cdot Y_{APF}(s)$ is an eigenvalue of $\boldsymbol{L}(s)$ corresponding to the same eigenvector $\boldsymbol{x}_\lambda(s)$. In other words, $\boldsymbol{L}(s)$ and $\boldsymbol{Z}_{SST}(s)$ have the same eigenvectors, and their eigenvalues are just weighted by the transfer function $Y_{APF}(s)$ of the APF controller.

Given the symmetry property (4), $\boldsymbol{Z}_{SST}(s)$ only has two distinct eigenvalues $Z_{\lambda,1}(s)$ and $Z_{\lambda,2}(s)$, expressed as:

$$Z_{\lambda,1}(s) = Z_A(s) - Z_M(s) \tag{16}$$

$$Z_{\lambda,2}(s) = Z_A(s) + (N-1) \cdot Z_M(s) \tag{17}$$

(with $Z_{\lambda,1}(s)$ having multiplicity $(N-1)$, and $Z_{\lambda,2}(s)$ having multiplicity 1). The analytical derivation of (16)-(17) is provided in the Appendix. As can be noted, $Z_{\lambda,1}(s)$ only depends on the difference between $Z_A(s)$ and $Z_M(s)$, while $Z_{\lambda,2}(s)$ also depends on the number of modules N of the ISOP SST. This means that, the higher is the mutual impedance and the number of modules, the stronger is the coupling existing between different APFs in operation.

Therefore, from (15), the stability of the overall ISOP SST with the presence of all N APFs can be assessed by analyzing the Nyquist plot of the two open-loop transfer functions:

$$L_{\lambda,1}(s) = Z_{\lambda,1}(s) \cdot Y_{APF}(s) \tag{18}$$

$$L_{\lambda,2}(s) = Z_{\lambda,2}(s) \cdot Y_{APF}(s) \tag{19}$$

meaning that $Z_{\lambda,1}(s)$ and $Z_{\lambda,2}(s)$ behave as equivalent impedances for the overall ISOP SST.

To summarize, the transfer function $Y_{APF}(s)$ should not only be verified towards the impedance $Z_A(s)$ of a single SST module, but also towards the equivalent impedances $Z_{\lambda,1}(s)$ and $Z_{\lambda,2}(s)$ of the overall coupled system. If compared to the analysis of (12)-(13), this approach drastically simplifies the evaluation of the stability of the SST, which can also be helpful in improving a more robust design.

IV. Evaluation of the ISOP SST Impedances

A. Experimental Setup

The experimental setup adopted in this work is a single-phase ISOP SST based on the low voltage prototype of the Power Electronic Traction Transformer (PETT) described in [5] and represented in Fig. 2. This converter is currently used as a research platform to analyze and improve the design and the control software development for ISOP SST converters.

The circuit architecture of the PETT, schematically represented in Fig. 2), is composed of $N = 9$ identical modules, each of which includes a non-isolated AC/DC conversion stage and a galvanically isolated DC/DC conversion stage.

In the considered setup, the isolated DC/DC conversion stages are realized with an LLC Series Resonant Conversion architecture, implemented with a half-bridge leg and a split-capacitor. The primary-side half-bridge legs are operated in open-loop with a 50% duty-cycle modulation at a frequency slightly lower than the resonance frequency of the LLC tank, in order to achieve soft-switching operation [4]–[6].

The AC/DC conversion stages are based on a full-bridge architecture. They are operated in closed-loop to control the

This article has been accepted for publication in IEEE Transactions on Power Electronics. This is the author's version which has not been fully edited and content may change prior to final publication. Citation information: DOI 10.1109/TPEL.2024.3351314

TABLE I
USED PARAMETERS OF THE PETT

Parameter		Value
Rated Power	P	8 kW
AC Grid Voltage (RMS)	$V_{AC,RMS}$	800 V
AC Grid Frequency	f_{AC}	50 Hz
Number of ISOP Modules	N	9
Primary DC Voltage (single module)	V_{DC}	220 V
Primary DC Capacitance (single module)	$C_{p,LLC}$	375 µF
Secondary DC Voltage	$V_{DC,out}$	220 V
Secondary DC Capacitance (equivalent)	$C_{s,LLC}$	680 µF
LLC Resonant Inductance	L_{res}	135 µH
LLC Resonant Capacitance	C_{res}	60 µF
LLC Magnetizing Inductance	L_{mag}	13 mH
LLC Transformation Ratio	N_1/N_2	1
AC/DC Switching Frequency	$f_{AC/DC}$	317 Hz
DC/DC Switching Frequency	$f_{DC/DC}$	1.5 kHz
APF Apparent Power	S_{APF}	1 kVA
APF Buck Inductance	L_{APF}	200 µH
APF Buck Capacitance	C_{APF}	360 µF
APF Buck Capacitor Voltage (DC offset)	V_C^*	160 V
APF DC-bus Capacitance	$C_{p,APF}$	120 µF
APF Switching Frequency	$f_{sw,APF}$	10 kHz

AC grid current in a way to transfer, with unitary power factor, a desired power flow. The transferred power is itself obtained from a closed-loop controller with the aim of stabilizing the DC-bus voltage on the secondary side of the overall ISOP SST. A phase shift pulse width modulation is implemented to control the full-bridge converters. With this technique, by shifting the carrier of the 9 modules by $1/9$ of their period, it is possible to improve the harmonic content of the equivalent voltage generated on the AC side, despite the relatively low switching frequency. At the same time, the switching harmonics generated by the AC/DC converters on the DC-bus currents of the 9 modules, once combined at the parallel output of the ISOP structure, cancel one another, meaning that the switching harmonics do not propagate to the secondary side of the SST [4]–[7].

The parameters of the PETT are summarized in Table I.

A Buck-type second-order harmonic active power filter has been installed in each of the 9 floating DC-buses of the PETT, as represented in the circuit diagram of Fig. 2. The main parameters of the APFs are also provided in Table I.

As described in [7], the presence of the APFs allowed the reduction of the primary-side DC-bus capacitance of each ISOP module from 4 mF to 375 µF, and the reduction of the secondary-side DC-bus capacitances from 2.35 mF to 680 µF. Indeed, thanks to the APFs, the DC-bus capacitances do not need to be sized for the suppression of the second-order harmonic ripple, and is instead only subject to the switching harmonics produced by the conversion stages of the SST.

For all the further analysis, the 9 APFs have been controlled to implement the same transfer function $Y_{APF}(s)$, and each reference current $i_{APF,k}$ has been computed based solely on the measurement of the local DC-bus voltage $v_{DC,k}$. This current reference is then tracked by a low-level controller of the buck-type circuit, which operates based on the control of the instantaneous energy stored in the APF capacitor C_{APF}. Additional details about the hardware and the low-level control software can be found in [5], [7].

B. Evaluation of the Equivalent Impedances

To analyze the system stability using the approach developed in this work, it is first necessary to know the impedance matrix $\boldsymbol{Z}_{SST}(s)$ of the ISOP SST.

To do that, it is possible to refer to the equivalent circuit represented in Fig. 3. In this equivalent circuit, initially developed in [14], the AC/DC stages are modeled as simple current sources injecting the second-order harmonic ripple to the system, the DC load is modeled as a purely resistive element, and the LLC conversion stages are modeled with a Π circuit consisting of two shunt capacitors and an ohmic-inductive branch.

Considering the split-capacitor configuration of the analyzed system, the equivalent capacitances of each module are one half of the installed capacitance at the primary-side and secondary-side of the LLC converters. For the primary side, the equivalent capacitance C_p takes also into account the contribution of the local DC-bus capacitance of the APF.

The equivalent inductance and resistance of the LLC converter identify the equivalent stored energy and the equivalent losses of the DC/DC conversion stage, respectively [15]. For a split-capacitor configuration they can be approximated as:

$$L_{DC} \approx L_{res} \cdot \left(\pi f_{res}/f_{sw,DC/DC}\right)^2 \tag{20}$$

$$R_{DC} \approx R_{res} \cdot \left(\pi^2/2\right) \cdot \left(f_{res}/f_{sw,DC/DC}\right) \tag{21}$$

with R_{res} taking into account the overall resistance of the LLC converter, and $f_{res} = 1/(2\pi\sqrt{L_{res}C_{res}})$ being the resonance frequency of the converter [15]. In the considered setup, $L_{DC} \approx 1.85\,\mathrm{mH}$ and $R_{DC} \approx 1\,\Omega$.

The analytical expressions of $Z_A(s)$ and $Z_M(s)$ obtained from the analysis of this equivalent circuit are reported in (22)-(23). Fig. 4 shows the magnitude and phase diagrams of the self-impedance Z_A and of the mutual impedance Z_M for varying frequencies, obtained considering $s = j\omega$ in (22)-(23).

It can be noted how both impedances show a resonant behavior, caused by the interaction between the DC-bus ca-

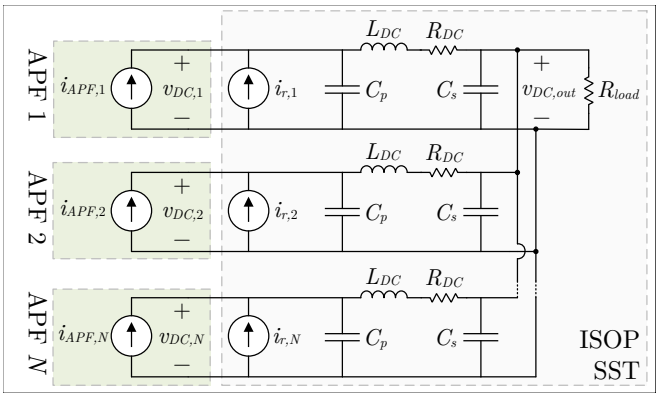

Fig. 3. Simplified equivalent circuit to analyze the PETT as a MIMO system.

This article has been accepted for publication in IEEE Transactions on Power Electronics. This is the author's version which has not been fully edited and content may change prior to final publication. Citation information: DOI 10.1109/TPEL.2024.3351314

pacitors and the equivalent inductance of the LLC converters. Additionally, the phase diagram of Z_A shows both positive and negative values, indicating that for some frequencies the system behavior is dominated by the DC-bus capacitors, while for other frequencies it is dominated by the inductive behavior of the LLC conversion stages.

For the considered system parameters, it can be verified that the effect of different loading conditions (i.e., obtained by varying R_{load} in (22)-(23)) is completely negligible above 10 Hz, and therefore it does not play a significant role in the following stability analysis.

From the knowledge of $Z_A(s)$ and $Z_M(s)$, using (16)-(17), it is possible to compute the eigenvalues $Z_{\lambda,1}(s)$ and $Z_{\lambda,2}(s)$ of the SST impedance matrix $\boldsymbol{Z}_{SST}(s)$. Fig. 5 shows their magnitude and phase diagrams for varying frequency, and compares it to the corresponding diagrams of $Z_A(s)$.

As can be noted, while $Z_{\lambda,1}(s)$ closely resembles $Z_A(s)$ for a wide frequency range (i.e., from around 20 Hz on), the eigenvalue $Z_{\lambda,2}(s)$ is sensibly different from $Z_A(s)$ until a much higher frequency (i.e., around 200 Hz). As shown in the following, the sensible difference in the phase diagrams of these equivalent impedances around 100 Hz has a dominant role on the stability of the closed loop system.

V. Experimental Results

A. Analyzed Test Scenarios

According to the previous analysis, the stability of the system when a single APF is operating can be assessed from the open-loop transfer function $L_A(s) = Z_A(s) \cdot Y_{APF}(s)$, while the stability of the SST considering the simultaneous operation of all APFs can be analyzed by referring to the two open-loop transfer functions $L_{\lambda,1}(s) = Z_{\lambda,1}(s) \cdot Y_{APF}(s)$ and $L_{\lambda,2}(s) = Z_{\lambda,2}(s) \cdot Y_{APF}(s)$.

To validate the proposed approach and show the importance of simultaneously observing the effect on $L_A(s)$, $L_{\lambda,1}(s)$ and $L_{\lambda,2}(s)$, two test scenarios are analyzed in the following.

In the first test, all the APFs have been programmed to emulate the transfer function:

$$Y_{APF,a}(s) = \frac{K_1 s}{s^2 + \omega_0^2} \tag{24}$$

with $K_1 = 1.5$ and $\omega_0 = 2\pi \cdot 100$ Hz.

In the second test, they have instead been programmed to emulate the transfer function:

$$Y_{APF,b}(s) = \frac{s(K_1 - s\,K_2)}{s^2 + \omega_0^2} \tag{25}$$

with $K_1 = 1.5$, $K_2 = 8.6 \cdot 10^{-3}$ and $\omega_0 = 2\pi \cdot 100$ Hz.

Both transfer functions include an ideal resonant term at the frequency of 100 Hz, in a way to provide an infinite gain to ideally cancel out the second-order harmonic ripple introduced by the AC/DC converters. They are both designed in a way that their magnitudes rapidly decay by moving away from 100 Hz, in order to be very selective on a single frequency component. However, compared to the transfer function $Y_{APF,a}(s)$ provided in (24), the transfer function $Y_{APF,b}(s)$ given in (25) also introduces a phase lag at the resonance frequency.

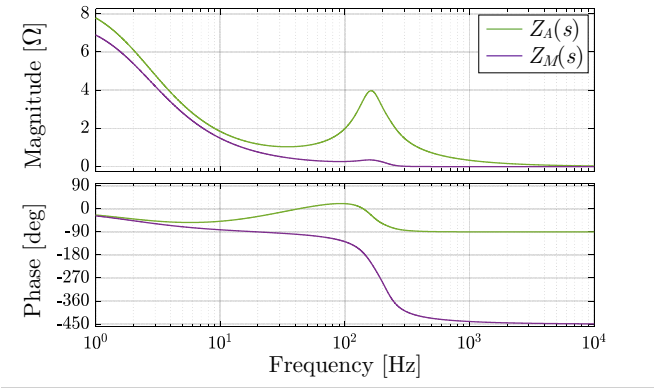

Fig. 4. Magnitude and phase diagram of the self-impedance $Z_A(s)$ and of the mutual impedance $Z_M(s)$ of the PETT for varying frequency, considering nominal loading conditions and including the DC-bus capacitance of the APFs.

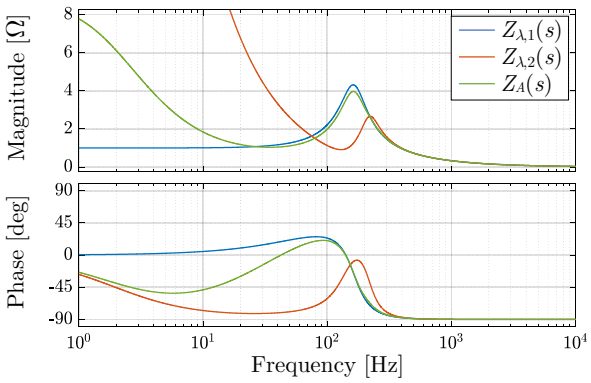

Fig. 5. Magnitude and phase diagram of the eigenvalues $Z_{\lambda,1}(s)$ and $Z_{\lambda,2}(s)$ of the SST impedances matrix $\boldsymbol{Z}_{SST}(s)$ for varying frequency. The self-inductance $Z_A(s)$ is also shown for comparison.

$$Z_A(s) = \cfrac{1}{sC_p + \cfrac{1}{sL_{DC} + R_{DC} + \cfrac{1}{(N-1)/Z_b(s) + N\,sC_s + 1/R_{load}}}} \quad \text{with} \quad Z_b(s) = sL_{DC} + R_{DC} + \frac{1}{sC_p} \tag{22}$$

$$Z_M(s) = Z_A(s) \cdot \frac{1/sC_p}{Z_b(s)} \cdot \frac{1}{(N-1)/Z_b(s) + N\,sC_s + 1/R_{load}} \cdot \cfrac{1}{sL_{DC} + R_{DC} + \cfrac{1}{(N-1)/Z_b(s) + N\,sC_s + 1/R_{load}}} \tag{23}$$

This article has been accepted for publication in IEEE Transactions on Power Electronics. This is the author's version which has not been fully edited and content may change prior to final publication. Citation information: DOI 10.1109/TPEL.2024.3351314

B. Results with $Y_{APF,a}(s)$

Considering the expression of $Y_{APF,a}(s)$ provided in (24), and the expressions of $Z_A(s)$, $Z_{\lambda,1}(s)$ and $Z_{\lambda,2}(s)$ found in the previous section, the expressions of $L_A(s)$, $L_{\lambda,1}(s)$ and $L_{\lambda,2}(s)$ can be easily computed. Their Bode diagrams and Nyquist diagrams are represented in Fig. 6.

For representation clarity, only positive frequencies are shown in the Nyquist diagram. Additionally, the presence of the resonant term in $Y_{APF,a}(s)$ introduces a couple of poles on the imaginary axis, and the the Nyquist plot is completed through additional branches with infinite radius, represented by the dashed traces in Fig. 6.

As can be noted from the Bode diagrams, all the open loop transfer functions have a very small magnitude in all frequency range, except in close proximity of 100 Hz, which is in line with the strict selectivity requirement of the APFs. This allows to simplify the analysis by focusing on the phase behavior close to the resonance, where the imaginary poles introduce a $-180°$ jump in the phase diagram.

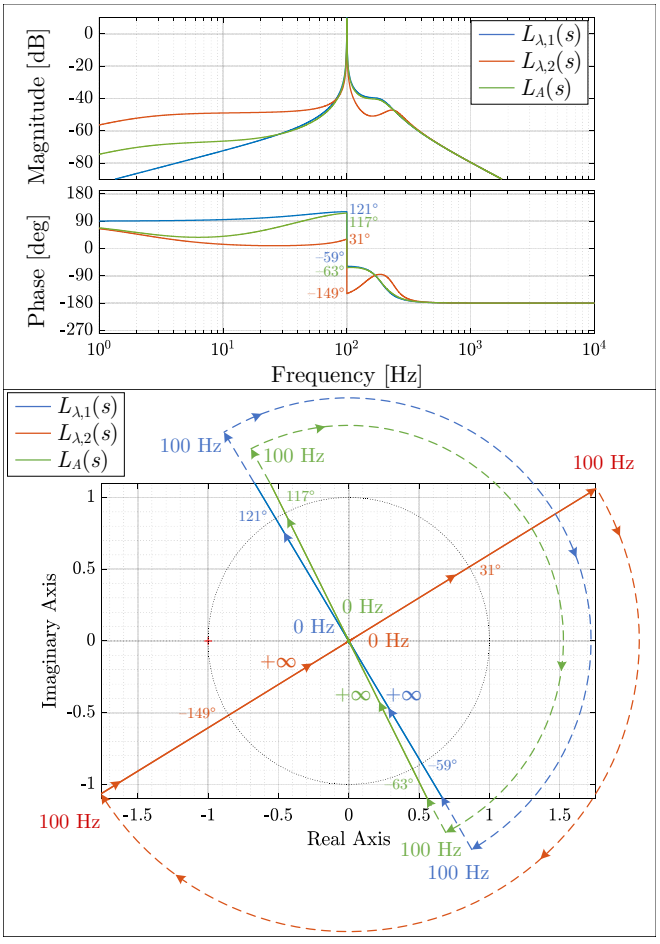

Fig. 6. Bode diagram (Top) and Nyquist diagram (Bottom) of the open-loop transfer functions $L_{\lambda,1}(s)$, $L_{\lambda,2}(s)$ and $L_A(s)$, considering the APF admittance $Y_{APF,a}(s)$ given in (24). In the Nyquist diagrams, only positive frequencies are shown. The dashed lines represent the behavior at infinite magnitude radius (obtained in proximity of poles on the imaginary axis).

By first focusing on the behavior of the system with a single APF in operation, it can be noted that the phase diagram of $L_A(s)$ is around $117°$ when approaching 100 Hz, and then jumps to $-63°$. From the Nyquist diagram it can be seen that the plot does not encircle the critical point $-1+j0$, meaning that the closed-loop system is asymptotically stable, with a phase margin of around $180° - 63° = 117°$.

To prove this result, Fig. 7 shows the experimental waveforms collected during the activation of a single APF controller (on the ISOP module 1). The left subplots of the figure show the measured current $i_{APF,1}$ injected by the APF on the SST module 1, the DC-bus voltage $v_{DC,1}$ on the same module, the DC-bus voltage $v_{DC,2}$ on one of the other modules, and the secondary-side voltage $v_{DC,out}$ of the overall SST. The right subplots of Fig. 7, denoted with the superscript $*^{\langle 2 \rangle}$, show the evolution of the magnitude of the harmonic components at the 100 Hz frequency, computed using a time-varying Fourier decomposition in a moving time window of 50 ms.

As can be noted, after the APF activation (at around 0.25 s), the current $i_{APF,1}$ increases, while the ripple on $v_{DC,1}$ is counteracted, and the corresponding second-order harmonic component is almost completely neutralized in around 3 s. Relatively small effects can be seen on $v_{DC,2}$ and $v_{DC,out}$.

Fig. 8 shows the steady-state waveforms of the same variables (left plots), and the corresponding harmonic spectra (right plots). As can be noted, the DC-bus voltage $v_{DC,1}$ shows almost no harmonic ripple around 100 Hz, thanks to the operation of the APF. The presence of other harmonics at relatively low frequency in $v_{DC,1}$, $v_{DC,2}$ and $i_{APF,1}$ is primarily due to the low switching frequency of the AC/DC converters (i.e., 317 Hz). Thanks to the phase-shift modulation of the AC/DC stages, these harmonics are not propagated to the secondary-side of the SST [5]–[7]. However, it is worth noting that their presence does not impact the stability analysis presented in this work.

To investigate the system stability when all APFs are simultaneously enabled, the open-loop transfer functions $L_{\lambda,1}(s)$ and $L_{\lambda,2}(s)$ can be analyzed in the same way, by referring to the Bode diagrams and Nyquist diagrams of Fig. 6.

With the considered parameters, $L_{\lambda,1}(s)$ shows a very similar behavior to $L_A(s)$, and its phase diagram jumps from around $121°$ to around $-59°$ when crossing 100 Hz, providing a phase margin of around $180° - 59° = 121°$. On the contrary, $L_{\lambda,2}(s)$ shows a quite different phase behavior, that jumps from around $31°$ to around $-149°$ when crossing 100 Hz , resulting in a smaller phase margin of just around $180° - 149° = 31°$. Nevertheless, also in this case the Nyquist plot does not encircle the critical point $(-1+j0)$. Therefore, since both $L_{\lambda,1}(s)$ and $L_{\lambda,2}(s)$ are stable, from the previous analysis it can be inferred that, with the transfer function $Y_{APF,a}(s)$, the system is asymptotically stable also when all APFs are enabled at the same time.

To verify this result, Fig. 9 shows the experimental results obtained by simultaneously activating all 9 APFs of the system, while Fig. 10 shows the corresponding steady-state waveforms and harmonic spectra. As can be noted, the system

This article has been accepted for publication in IEEE Transactions on Power Electronics. This is the author's version which has not been fully edited and content may change prior to final publication. Citation information: DOI 10.1109/TPEL.2024.3351314

is asymptotically stable, and the second-order ripple on all the DC-bus voltages is properly neutralized, showing only some small residual components due to system non-idealities. However, in this case, the dynamic response of the system is slowed down compared to Fig. 7, and the steady state is only reached after several seconds.

C. Results with $Y_{APF,b}(s)$

Similarly to the previous test case, the expressions of $L_A(s)$, $L_{\lambda,1}(s)$ and $L_{\lambda,2}(s)$ can be immediately found from the knowledge of the system equivalent impedances and of the controller transfer function $Y_{APF,b}(s)$ given in (25). Their Bode and Nyquist diagrams are represented in Fig. 11.

By observing the behavior of $L_A(s)$ it can be seen that, once again, the magnitude of its frequency response is very small for all frequencies, except in proximity of 100 Hz. In this case, when crossing the resonance frequencies, the phase diagram jumps from around $42°$ to around $-138°$, resulting in a phase margin of around $180° - 138° = 42°$. Similarly to the previous case, the Nyquist diagram of $L_A(s)$ does not encircle the critical point $(-1 + j0)$, meaning that the system is asymptotically stable when a single APF is in operation.

To prove this result, Fig. 12 shows the experimental waveforms of the system collected during the activation of a single APF implementing $Y_{APF,b}(s)$, while Fig. 13 shows the corresponding steady-state waveforms and harmonic spectra.

As can be noted, the system is asymptotically stable and, compared to Fig. 7, it even shows a faster dynamic response after the activation, reaching steady state in around 1.5 s. The faster performances of $Y_{APF,b}(s)$ compared to $Y_{APF,a}(s)$ can be motivated by the presence of the phase lag in (25), which compensate the phase lead of $Z_A(s)$.

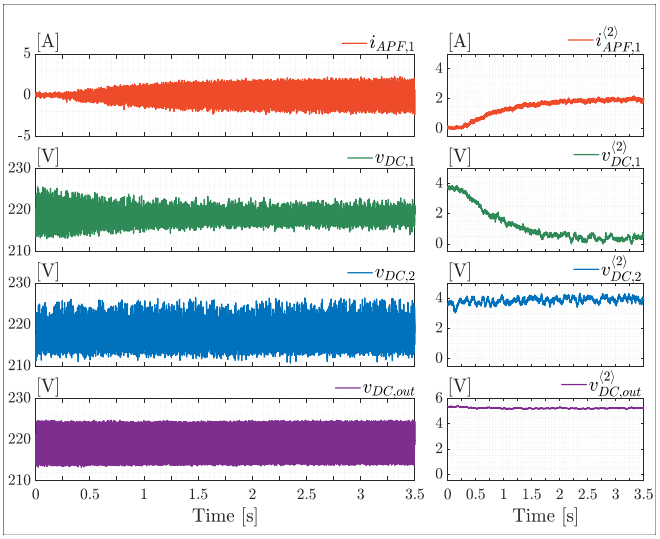

Fig. 7. Experimental results showing the activation of a single APF with the equivalent admittance $Y_{APF,a}(s)$.

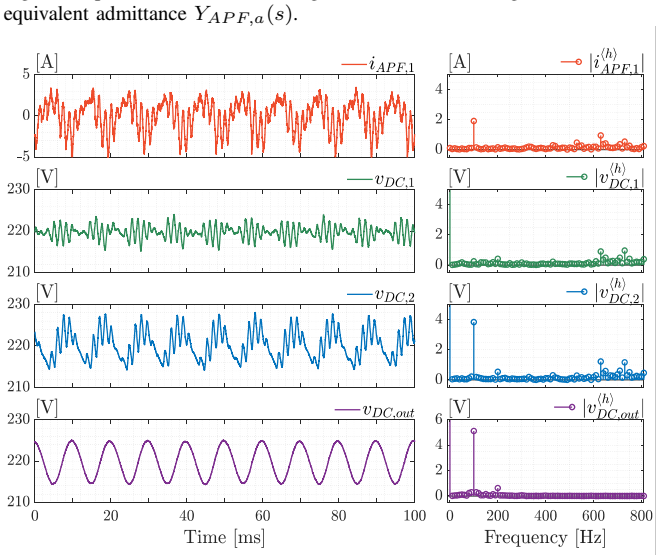

Fig. 8. Steady-state results following the activation of a single APF with the equivalent admittance $Y_{APF,a}(s)$.

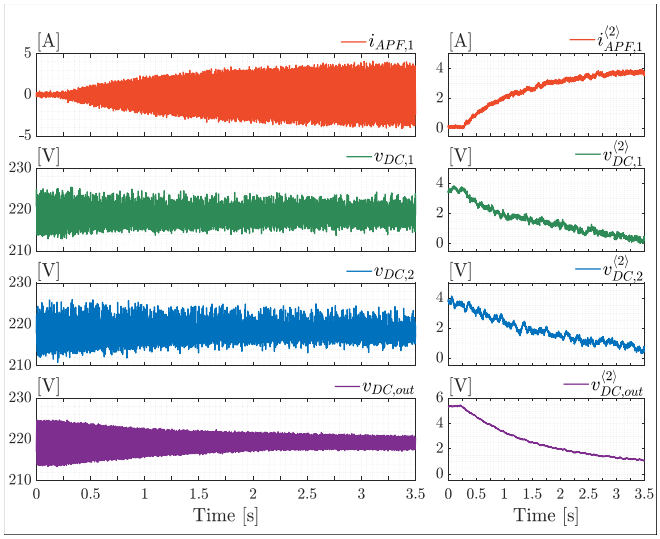

Fig. 9. Experimental results showing the simultaneous activation of all APFs with the equivalent admittance $Y_{APF,a}(s)$.

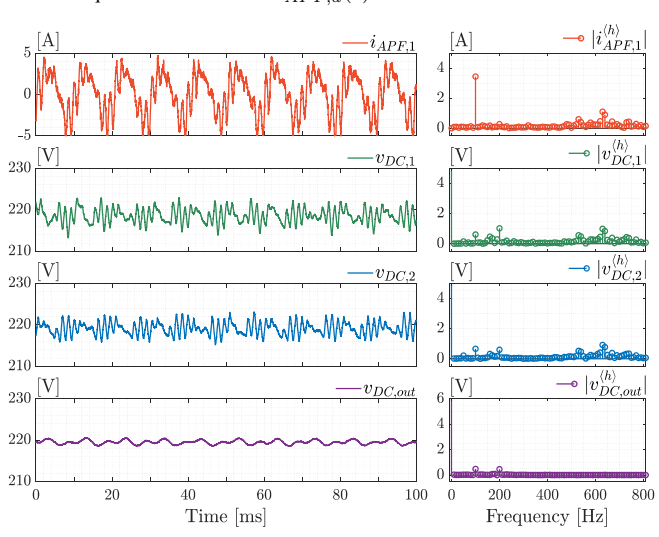

Fig. 10. Steady-state results following the simultaneous activation of all APFs with the equivalent admittance $Y_{APF,a}(s)$.

This article has been accepted for publication in IEEE Transactions on Power Electronics. This is the author's version which has not been fully edited and content may change prior to final publication. Citation information: DOI 10.1109/TPEL.2024.3351314

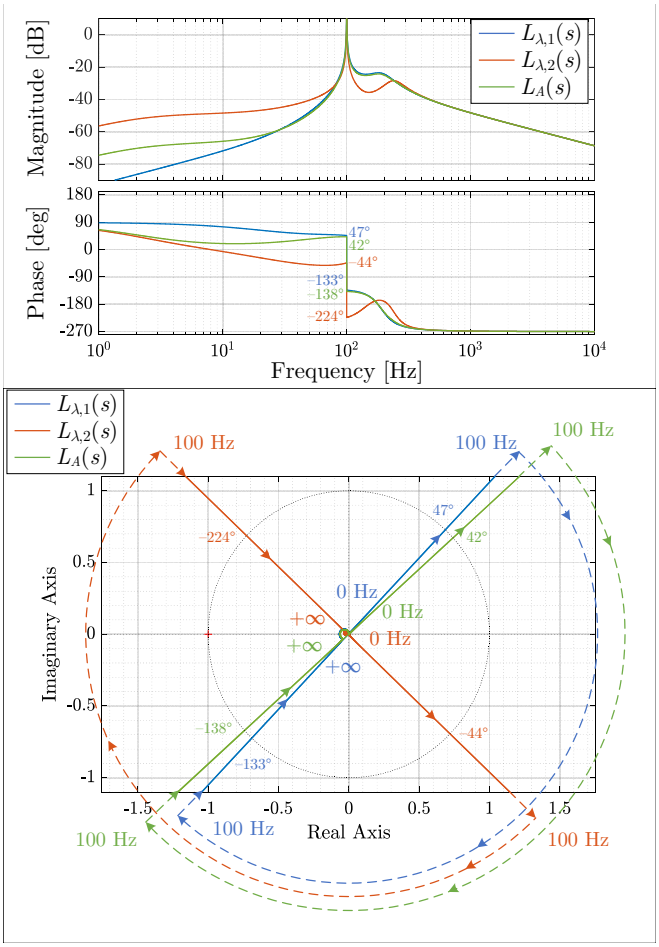

Fig. 11. Bode diagram (Top) and Nyquist diagram (Bottom) of the open-loop transfer functions $L_{\lambda,1}(s)$, $L_{\lambda,2}(s)$ and $L_A(s)$, considering the APF admittance $Y_{APF,b}(s)$ given in (25). In the Nyquist diagrams, only positive frequencies are shown. The dashed lines represent the behavior at infinite magnitude radius (obtained in proximity of poles on the imaginary axis).

The steady-state waveforms of Fig. 13 are also similar to the ones of Fig. 8.

Therefore, from the results of Fig. 12 and Fig. 13, one may erroneously assume that $Y_{APF,b}(s)$ would also be stable when implemented in all modules. However, the frequency responses of $L_{\lambda,1}(s)$ and $L_{\lambda,2}(s)$ show a considerable difference compared to the previous case. Indeed, while the frequency response of $L_{\lambda,1}(s)$ is similar to the one of $L_A(s)$ (jumping from around $47°$ to around $-133°$ when crossing $100\,\text{Hz}$ with a phase margin of around $47°$), the frequency response of $L_{\lambda,2}(s)$ considerably differs in the phase diagram, which jumps from around $-44°$ to around $-224°$ when crossing $100\,\text{Hz}$, resulting in a negative phase margin of around $-44°$.

As can be noted from the Nyquist diagram, while $L_{\lambda,1}(s)$ does not encircle the critical point $(-1+j0)$, $L_{\lambda,2}(s)$ shows one encirclement caused by the path of infinite radius. Therefore, in this case, the stability analysis based on the eigenvalues of the impedance matrix infers that the closed-loop system with all APFs in simultaneous operation is unstable.

To verify this result, Fig. 14 shows the experimental waveforms obtained during the simultaneous activation of all APF units implementing the transfer function $Y_{APF,b}(s)$. To safeguard the integrity of the laboratory equipment, this test has been executed in light loading conditions (i.e., less than $1\,\text{kW}$). As can be noted, immediately after the activation of the APFs (at around $0.25\,\text{s}$), the waveforms of $v_{DC,1}$, $v_{DC,2}$ and $i_{APF,1}$ start oscillating with an exponentially increasing magnitude, proving the unstable behavior of the system, until they reach the threshold levels causing their deactivation.

Despite this example has been intentionally designed to emphasize the potential instabilities caused by the internal couplings of the ISOP SST modules, it can be useful to warn about the possible dangers in developing conclusions based on the observation of a single APF unit working independently

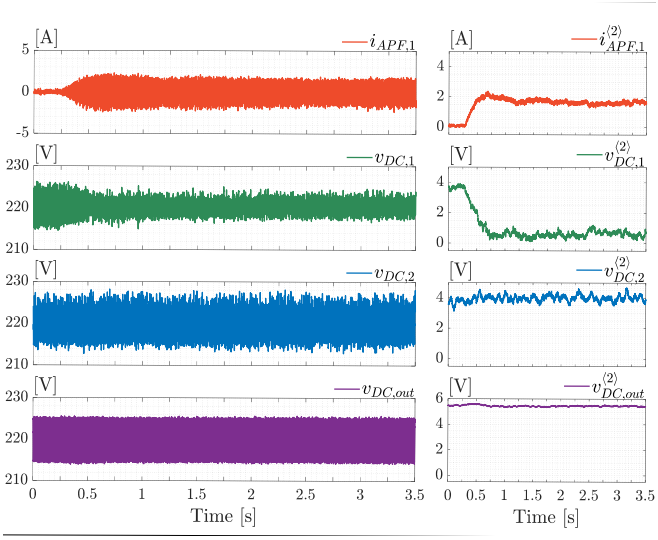

Fig. 12. Experimental results showing the activation of a single APF with the equivalent admittance $Y_{APF,b}(s)$.

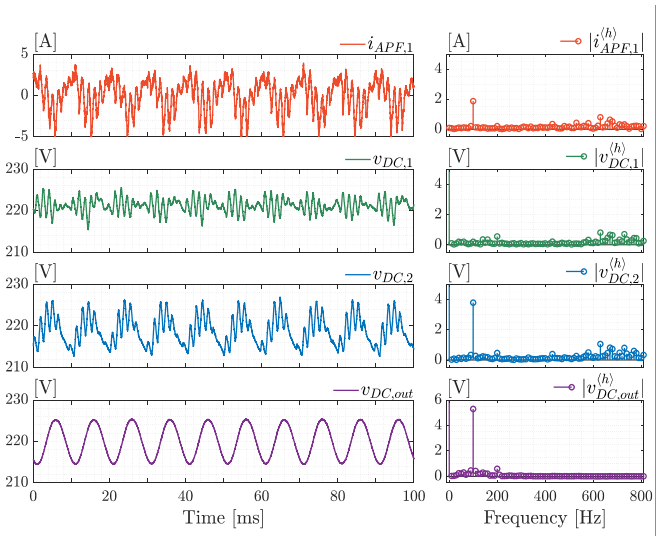

Fig. 13. Steady-state results following the activation of a single APF with the equivalent admittance $Y_{APF,b}(s)$.

This article has been accepted for publication in IEEE Transactions on Power Electronics. This is the author's version which has not been fully edited and content may change prior to final publication. Citation information: DOI 10.1109/TPEL.2024.3351314

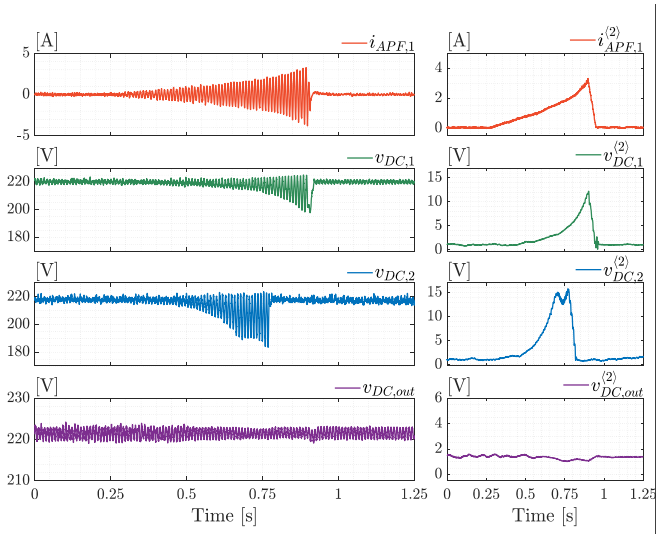

Fig. 14. Experimental results showing the simultaneous activation of all APFs with the equivalent admittance $Y_{APF,b}(s)$.

from the others. Indeed, in attempt to improve the dynamic behavior of a single APF, one could be tempted to add a phase compensation based on the angle of $Z_A(s)$ in proximity of ω_0 (e.g., around 100 Hz). However, by doing so, the phase diagrams of $L_{\lambda,1}(s)$ and $L_{\lambda,2}(s)$ would also be affected, potentially leading to destructive results.

Therefore, to guarantee a robust behavior, the APF controller should be designed taking into account the mutual coupling effects in the ISOP SST, which may be more or less relevant according to the system topology and parameters.

It is also important to point out that, in practical implementation, the real transfer function $Y_{APF}(s)$ obtained by the APFs can differ from the desired one implemented via software, since it may be altered by other dynamical effects, like the low-level controller and/or filters in the hardware measurement chain. These effects, which have not been explicitly modeled in the previous analysis, may also need to be considered to provide adequate stability margins to the system.

VI. Conclusions

ISOP SST converters suffer a second-order harmonic ripple caused by a local single-phase AC/DC conversion on each module. This ripple can be neutralized through active power filters. However, when multiple APFs are connected to the system, mutual interactions may arise between them, caused by coupling between different modules of the ISOP configuration, which could potentially lead to instability.

The main contributions of this work are the analysis of the dynamic interactions between the SST and the APFs through a Multi-Input/Multi-Output system formulation and the development of a simple and effective approach to assess the stability, based on the Generalized Nyquist Criterion.

It has first been shown that guaranteeing the stability of a single APF in operation is not enough to automatically guarantee a stable behavior when multiple APFs are enabled at once. Instead, the ISOP SST equipped with APFs should be analyzed as a MIMO dynamical system, explicitly considering the coupling among different modules.

Then, by using the GNC for MIMO dynamical systems, it has been shown that the stability can be analyzed with respect to two equivalent impedances of the system, computed as the eigenvalues of the overall impedance matrix of the SST. These equivalent impedances take into account both the self-induced effect of a single module and the mutual interaction between different modules in the ISOP configuration.

Therefore, the closed-loop stability of the overall ISOP SST can be assessed by the simultaneous stability of the APFs with respect to them. This provides a simple tool to analyze the closed-loop behavior of the system, which can be helpful for the design of the control algorithm of the APFs.

The results have been particularized and verified on a single-phase ISOP SST prototype.

Appendix

This section describes the analytical derivation of the eigenvalues of $\boldsymbol{Z}_{SST}(s)$, expressed by (16)-(17), and discusses properties of the corresponding eigenvectors. For notation compactness, in what follows, the dependence on the Laplace complex variable s will be omitted.

The eigenvalues of $\boldsymbol{Z}_{SST}$ can be found as the roots of its characteristic polynomial, which can itself be computed as the determinant of the matrix $(Z_\lambda \boldsymbol{I} - \boldsymbol{Z}_{SST})$ (with Z_λ denoting the unknown variable and $\boldsymbol{I}$ being the $N \times N$ identity matrix).

By using the expression (4) of $\boldsymbol{Z}_{SST}$, the characteristic polynomial can be expressed as in (26).

As known, the determinant of a matrix is unaltered if some of its rows are summed by linear combinations of other rows. Then, the expression (26) can be transformed in the expression (27) by subtracting the last row of the matrix from all the previous $(N-1)$ rows.

In a similar way, the determinant of a matrix is unaltered if some of its columns are summed by linear combinations of other columns. Then, the expression (27) can be further simplified and can be transformed in the expression (28) by summing all the first $(N-1)$ columns to the last one.

Finally, the resulting matrix in (28) is a triangular matrix, and its determinant can be computed by multiplying all its diagonal terms, resulting in the expression of (29).

The roots of the characteristic polynomial of $\boldsymbol{Z}_{SST}$ can be found by equalizing (29) to zero and by solving in terms of the unknown Z_λ. The results are immediately found to be $Z_{\lambda,1} = (Z_A - Z_M)$ and $Z_{\lambda,2} = (Z_A + (N-1) \cdot Z_M)$, which are the expressions of the eigenvalues provided in (16)-(17).

In particular, from (29), it can be seen that $(Z_A - Z_M)$ appears $(N-1)$ times as the root of the characteristic polynomial, meaning that the eigenvalue $Z_{\lambda,1}$ has algebraic multiplicity equal to $(N-1)$. On the contrary, $(Z_A + (N-1) \cdot Z_M)$ appears only once as the root of the characteristic polynomial, and the eigenvalue $Z_{\lambda,2}$ has algebraic multiplicity equal to 1.

Regarding $Z_{\lambda,2}$, its geometric multiplicity will necessarily be equal to 1 and, by direct substitution, it can be verified

$$\det(Z_\lambda \boldsymbol{I} - \boldsymbol{Z}_{SST}) = \det \begin{bmatrix} (Z_\lambda - Z_A) & -Z_M & -Z_M & \cdots & -Z_M \\ -Z_M & (Z_\lambda - Z_A) & -Z_M & \cdots & -Z_M \\ \vdots & \vdots & \vdots & \ddots & \vdots \\ -Z_M & -Z_M & -Z_M & \cdots & (Z_\lambda - Z_A) \end{bmatrix} = \tag{26}$$

$$= \det \begin{bmatrix} (Z_\lambda - Z_A + Z_M) & 0 & 0 & \cdots & -(Z_\lambda - Z_A + Z_M) \\ 0 & (Z_\lambda - Z_A + Z_M) & 0 & \cdots & -(Z_\lambda - Z_A + Z_M) \\ \vdots & \vdots & \vdots & \ddots & \vdots \\ -Z_M & -Z_M & -Z_M & \cdots & (Z_\lambda - Z_A) \end{bmatrix} = \tag{27}$$

$$= \det \begin{bmatrix} (Z_\lambda - Z_A + Z_M) & 0 & 0 & \cdots & 0 \\ 0 & (Z_\lambda - Z_A + Z_M) & 0 & \cdots & 0 \\ \vdots & \vdots & \vdots & \ddots & \vdots \\ -Z_M & -Z_M & -Z_M & \cdots & (Z_\lambda - Z_A - (N-1) \cdot Z_M) \end{bmatrix} = \tag{28}$$

$$= \big(Z_\lambda - Z_A + Z_M\big)^{N-1} \cdot \big(Z_\lambda - Z_A - (N-1) \cdot Z_M\big) \tag{29}$$

that the corresponding eigenvector is $\boldsymbol{x}_{\lambda,2} = [1, 1, 1, \ldots, 1]^{\mathrm{T}}$ (i.e., a $N \times 1$ vector with all terms equal to 1). Indeed, by multiplying $\boldsymbol{Z}_{SST}$ by $\boldsymbol{x}_{\lambda,2}$, the k-th element of the resulting vector will be equal to the sum of all elements in the k-th row of $\boldsymbol{Z}_{SST}$, which is equal to $(Z_A + (N-1) \cdot Z_M)$.

Regarding $Z_{\lambda,1}$, it can be verified that all the vectors $\boldsymbol{x}_{\lambda,1_1} = [1, -1, 0, \ldots, 0]^{\mathrm{T}}$, $\boldsymbol{x}_{\lambda,1_2} = [1, 0, -1, \ldots, 0]^{\mathrm{T}}$, $\ldots$, $\boldsymbol{x}_{\lambda,1_{N-1}} = [1, 0, 0, \ldots, -1]^{\mathrm{T}}$ satisfy the definition (14) (i.e., all $N \times 1$ vectors whose first element is equal to 1, with only another element equal to -1, and with all other elements being zero). Indeed, by multiplying $\boldsymbol{Z}_{SST}$ by any of these vectors, the first element of the result will be equal to $(Z_A - Z_M)$, the element corresponding to the -1 value will be equal to $-(Z_A + Z_M)$, and all other elements will be equal to zero.

Since all the $(N-1)$ eigenvectors $\boldsymbol{x}_{\lambda,1_1}, \boldsymbol{x}_{\lambda,1_2}, \ldots, \boldsymbol{x}_{\lambda,1_{N-1}}$ are linearly independent, the geometric multiplicity of $Z_{\lambda,1}$ is equivalent to its algebraic multiplicity and equal to $(N-1)$.

REFERENCES

[1] J. E. Huber and J. W. Kolar, "Solid-State Transformers: On the Origins and Evolution of Key Concepts," in IEEE Industrial Electronics Magazine, vol. 10, no. 3, pp. 19-28, Sept. 2016, doi: 10.1109/MIE.2016.2588878.

[2] E. R. Ronan, S. D. Sudhoff, S. F. Glover and D. L. Galloway, "A power electronic-based distribution transformer," in IEEE Transactions on Power Delivery, vol. 17, no. 2, pp. 537-543, April 2002, doi: 10.1109/61.997934.

[3] M. Liserre, G. Buticchi, M. Andresen, G. De Carne, L. F. Costa and Z. X. Zou,, "The Smart Transformer: Impact on the Electric Grid and Technology Challenges," in IEEE Industrial Electronics Magazine, vol. 10, no. 2, pp. 46-58, June 2016, doi: 10.1109/MIE.2016.2551418.

[4] N. Hugo, P. Stefanutti, M. Pellerin and A. Akdag, "Power electronics traction transformer," 2007 European Conference on Power Electronics and Applications, Aalborg, Denmark, 2007, pp. 1-10, doi: 10.1109/EPE.2007.4417649.

[5] D. Dujic et al., "Power Electronic Traction Transformer-Low Voltage Prototype," in IEEE Transactions on Power Electronics, vol. 28, no. 12, pp. 5522-5534, Dec. 2013, doi: 10.1109/TPEL.2013.2248756.

[6] C. Zhao et al., "Power Electronic Traction Transformer—Medium Voltage Prototype," in IEEE Transactions on Industrial Electronics, vol. 61, no. 7, pp. 3257-3268, July 2014, doi: 10.1109/TIE.2013.2278960.

[7] T. Wei, A. Cervone and D. Dujic, "Second Harmonic Ripple Voltage Suppression for Single-Phase ISOP Solid-State Transformer by Active Power Decoupling," 2023 IEEE Applied Power Electronics Conference and Exposition (APEC), Orlando, FL, USA, 2023, pp. 1496-1502, doi: 10.1109/APEC43580.2023.10131324.

[8] J. C. Das, "Passive filters - potentialities and limitations," in IEEE Trans. .Ind. Appl., vol. 40, no. 1, pp. 232-241, Jan.-Feb. 2004, doi: 10.1109/TIA.2003.821666.

[9] Y. Sun, Y. Liu, M. Su, W. Xiong and J. Yang, "Review of Active Power Decoupling Topologies in Single-Phase Systems," in IEEE Trans. Pow. Electron., vol. 31, no. 7, pp. 4778-4794, July 2016, doi: 10.1109/TPEL.2015.2477882.

[10] D. Neumayr, G. C. Knabben, E. Varescon, D. Bortis and J. W. Kolar, "Comparative Evaluation of a Full- and Partial-Power Processing Active Power Buffer for Ultracompact Single-Phase DC/AC Converter Systems," in IEEE Journ. Emerg. Select. Topics in Pow. Electron., vol. 9, no. 2, pp. 1994-2013, April 2021, doi: 10.1109/JESTPE.2020.2987937.

[11] Z. Qin, Y. Tang, P. C. Loh and F. Blaabjerg, "Benchmark of AC and DC Active Power Decoupling Circuits for Second-Order Harmonic Mitigation in Kilowatt-Scale Single-Phase Inverters," in IEEE Journ. Emerg. Select. Topics in Pow. Electron., vol. 4, no. 1, pp. 15-25, March 2016, doi: 10.1109/JESTPE.2015.2490199.

[12] R. Wang et al., "A High Power Density Single-Phase PWM Rectifier With Active Ripple Energy Storage," in IEEE Trans. Pow. Electron., vol. 26, no. 5, pp. 1430-1443, May 2011, doi: 10.1109/TPEL.2010.2090670.

[13] G. Jia, M. Chen, S. Tang, C. Zhang and G. Zhu, "Active Power Decoupling for a Modified Modular Multilevel Converter to Decrease Submodule Capacitor Voltage Ripples and Power Losses," in IEEE Trans. Pow. Electron., vol. 36, no. 3, pp. 2835-2851, March 2021, doi: 10.1109/TPEL.2020.3016493.

[14] A. Cervone, T. Wei and D. Dujic, "Coupling Dynamics of Second-Order Harmonic Active Filters in Single-Phase Input-Series/Output-Parallel AC-DC Converters," PCIM Europe 2023, Nuremberg, Germany, 2023, pp. 1-10, doi: 10.30420/566091033

[15] J. E. Huber, J. Minibock and J. W. Kolar, "Generic Derivation of Dynamic Model for Half-Cycle DCM Series Resonant Converters," in IEEE Trans. Pow. Electron., vol. 33, no. 1, pp. 4-7, Jan. 2018, doi: 10.1109/TPEL.2017.2703300.

[16] C. Desoer and Yung-Terng Wang, "On the generalized nyquist stability criterion," in IEEE Trans. Autom. Contr., vol. 25, no. 2, pp. 187-196, April 1980, doi: 10.1109/TAC.1980.1102280.